Published in Physics of Plasmas, **9,** pp 4309-4316 (2002).

# Reduction of enhanced edge emission in a large area electron beam

F. Hegeler
*Naval Research Laboratory, Plasma Physics Division, Code 6730, Washington, DC 20375*
*and Commonwealth Technology, Inc., 5875 Barclay DR, Alexandria, VA 22315*

M. Friedman, M.C. Myers, and J.D. Sethian
*Naval Research Laboratory, Plasma Physics Division, Code 6730, Washington, DC 20375*

S.B. Swanekamp
*Naval Research Laboratory, Plasma Physics Division, Code 6770, Washington, DC 20375*
*and TITAN/JAYCOR, McLean, VA 22102*

This paper presents measurements of the enhanced current density along the edges of a large area electron beam as well as successful techniques that eliminate this edge effect/beam halo. The spatial and temporal current density data is obtained with a Faraday cup array at the anode, and the spatial, time-integrated current density is obtained with radiachromic film. MAGIC particle-in-cell (PIC) simulations support the experimental results. Experiments and simulations show that recessing the cathode reduces the electric field at the edge and eliminates the edge effect. However the field shaper itself emits under long-term repetitive operation. In contrast using a floating metallic electric field shaper, which is electrically insulated from the cathode, eliminates the beam halo and prevents or minimizes electron emission from its surface during repetitive operation.

## I. INTRODUCTION

Electra is a repetitively pulsed, electron beam pumped krypton fluoride (KrF) laser that is used to develop the technology required for inertial fusion energy (IFE). A full scale fusion KrF laser will be pumped with electron beams with cross-sections of 2,500 to 10,000 $cm^2$. Understanding the mechanisms that govern uniform electron beam emission over large area cathodes is important for overall system efficiency and durability. It is well known that the current density is increased near the edges of planar explosive emission cathodes. This beam halo is caused by a discontinuity between the vacuum electric field outside the diode (see position 1 of Fig. 1a) and the electric field inside the diode where space-charge dominates the electric field. Recessing the cathode into a metallic shroud reduces the electric field to zero at the cathode edge and can eliminate the beam halo [1]. An example of this is shown in Fig. 1b. For relativistic e-beam applications with average electric fields on the order of 100 kV/cm, the elimination of the halo becomes more problematic since electron emission from the electric field shaper must also be suppressed.

This research is part of the Electra KrF laser program [2-3] with the goal to develop the technologies needed to produce an efficient and reliable, electron beam pumped laser that operates at 5 Hz continuously for 2 years. Elimination this beam halo is essential to the Electra laser program since the high current density in the halo significantly reduces the lifetime of the foil that separates the vacuum diode from the high-pressure laser gas. Simply blocking the beam edge with an aperture is not acceptable since this would significantly decrease the overall efficiency.

Section II presents the concept of recessed cathodes by simulating the beam halo in 2-D, which is then followed by a brief description of the experimental apparatus in Section III. Section IV provides experimental data from a Faraday cup array, and section V discusses global beam rotation and pinching with 3-D simulations and estimates the self-magnetic field of the electron beam. Section VI shows experimental results with and without a cathode recess and describes the limitation of the cathode recess concept. Section VII describes the successful use of a novel electrically insulated field shaper to remove the beam halo.

## II. SIMULATION OF THE BEAM HALO

Simulations of the current density along the edge of the electron beam have been performed using the MAGIC [4] 2-D PIC code. Since we were only interested in the edge physics, the cathode size was limited to 10 cm in the simulations. For all simulations, a voltage pulse of 500 kV with a risetime of 20 ns was used and the program was stopped after 50 ns when the simulated waveforms reached steady state. An axial magnetic field of 1.4 kG (0.14 T) is applied as in the experiments to minimize pinching of the electron beam in the self-magnetic field. The spatial variation of the current density was calculated along the surface of the anode. The following coordinate system is used in this paper: $x$ is the propagation direction of the electron beam, $y$ is the direction along the cathode (e.g., $y_{cathode}$ is 10 cm in the simulations and 27 cm in most of the experimental data), and $z$ is the horizontal direction of the cathode and the direction of propagation of the laser beam (see Fig. 1).

# Report Documentation Page

*Form Approved*
*OMB No. 0704-0188*



| 1. REPORT DATE | 2. REPORT TYPE | 3. DATES COVERED |
|---|---|---|
| **2002** | | **00-00-2002 to 00-00-2002** |

| 4. TITLE AND SUBTITLE | 5a. CONTRACT NUMBER |
|---|---|
| **Reduction of enhanced edge emission in a large area electron beam** | 5b. GRANT NUMBER |
| | 5c. PROGRAM ELEMENT NUMBER |
| 6. AUTHOR(S) | 5d. PROJECT NUMBER |
| | 5e. TASK NUMBER |
| | 5f. WORK UNIT NUMBER |
| 7. PERFORMING ORGANIZATION NAME(S) AND ADDRESS(ES) **Naval Research Laboratory,Plasma Physics Division,Code 6730,Washington,DC,20375** | 8. PERFORMING ORGANIZATION REPORT NUMBER |
| 9. SPONSORING/MONITORING AGENCY NAME(S) AND ADDRESS(ES) | 10. SPONSOR/MONITOR'S ACRONYM(S) |
| | 11. SPONSOR/MONITOR'S REPORT NUMBER(S) |

12. DISTRIBUTION/AVAILABILITY STATEMENT
**Approved for public release; distribution unlimited**

13. SUPPLEMENTARY NOTES

14. ABSTRACT

15. SUBJECT TERMS

| 16. SECURITY CLASSIFICATION OF: | | | 17. LIMITATION OF ABSTRACT | 18. NUMBER OF PAGES | 19a. NAME OF RESPONSIBLE PERSON |
|---|---|---|---|---|---|
| a. REPORT | b. ABSTRACT | c. THIS PAGE | | | |
| **unclassified** | **unclassified** | **unclassified** | **Same as Report (SAR)** | **8** | |

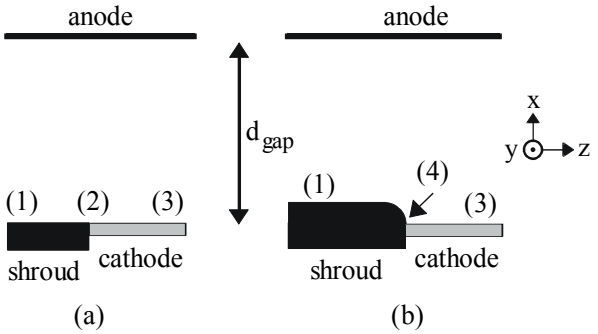


FIG. 1. Schematic of the A-K gap. (a) cathode surface is flush with the non-emitting cathode shroud. (1) vacuum electric field, (2) position of the e-beam halo, and (3) $E = 0$ during space-charge limited emission. (b) cathode is recessed to reduce the electric field to zero at position (4).

Figure 2 shows the dependence of the cathode recess depth $dx$ ranging from 0 to 10 mm for a cell grid size of 1 mm, and Table I provides the peak current density normalized to the Child-Langmuir current density ($J_{CL}$) for the first five cases. For recesses of more than 5 mm, the beam halo is eliminated but the spatial decrease in current density extends over more than 1 cm. For uniform pumping of the laser gas it is desirable that the profile have a sharp cut-off. The simulations indicate that a 2-4 mm recess is acceptable.

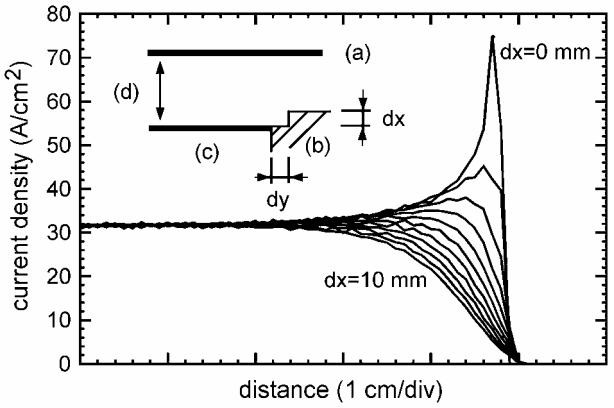


FIG. 2. Simulation of the e-beam halo with PIC code grid resolution of 1 mm. (a) anode, (b) metallic non emitting shroud, (c) cathode, and (d) A-K gap of 5 cm, with $dx$ ranging from 0 to 10 mm, and $dy$ = 1 mm for all cases.

Adequate resolution of the cathode edge is required to obtain good predictions of the beam halo current density [5]. With finer grid sizes the ratio of beam halo peak current density to Child-Langmuir current density ($J_{peak}/J_{CL}$) is larger than 3 without a cathode recess (see Fig. 3). For this simple 2-D simulation, finer grid sizes do not necessarily provide more numerically accurate answers because the features of the cathode edge are not modeled exactly. Table II shows that the beam halo width decreases at higher halo amplitudes. The FWHM of the halo includes only parts above the Child-Langmuir current density base line. Experimental data without a cathode recess shown in the following sections compared best to simulations with grid sizes of 1 to 2 mm. For cases when the cathode is recessed, the simulations show only small dependencies with the cell grid size (e.g., $J_{peak}/J_{CL}$ is 1.18 and 1.2 for grid resolutions of 0.5 and 1 mm, respectively). Thus, the PIC code becomes a useful tool for designing the shape of the cathode shroud.

TABLE I. Normalized beam halo peak current density for various cathode recess heights as shown in Figure 2.

| Cathode recess $dx$ (mm) | 0 | 1 | 2 | 3 | 4 |
|---|---|---|---|---|---|
| Normalized peak current density ($J_{peak}/J_{CL}$) | 2.4 | 1.4 | 1.2 | 1.1 | 1.06 |

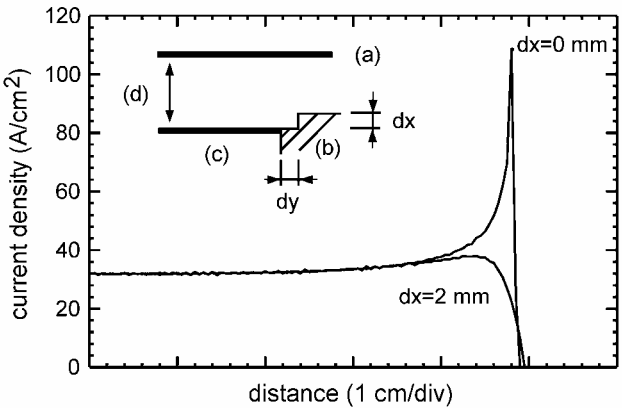


FIG. 3. Simulation of the e-beam halo with PIC code grid resolution of 0.5 mm. (a) anode, (b) metallic non emitting shroud, (c) cathode, and (d) A-K gap of 5 cm, and $dy$ = 0.5 mm. The normalized peak current density is 3.4 and 1.18 for $dx$ = 0 and 2 mm, respectively.

TABLE II. Normalized beam halo peak current density as a function of the PIC code grid resolution. The cathode is not recessed.

| Grid resolution (mm) | 0.25 | 0.5 | 1.0 | 2.5 | 5.0 |
|---|---|---|---|---|---|
| Normalized peak current density ($J_{peak}/J_{CL}$) | 3.2 | 3.4 | 2.4 | 1.8 | 1.8 |
| FWHM of the peak (mm) | 1 | 0.7 | 2.1 | 4.2 | 4.8 |

## III. EXPERIMENTAL SETUP

The basic experimental apparatus has been described previously [2, 6], therefore, it is only briefly summarized here. A capacitor bank that is switched through a 1:12 step-up auto-transformer charges two parallel water pulse-forming lines. Typical operating parameters are 400-550 kV, 70-110 kA, with A-K gaps of 4 to 6 cm. Two cathode sizes (27 x 97 and 35 x 106 cm$^2$) and various cathode materials have been tested. To minimize pinching, the e-beam is guided through the A-K gap by an axial magnetic field of 1.4 kG. This is roughly twice the amplitude of the self-magnetic field at peak current. The anode consists of a 2.5 cm thick aluminum plate covered with 6.3 mm Poco

graphite and a 25 μm thick aluminized Kapton foil with access ports for diagnostics. In this paper, all experimental results have been obtained with a velvet cathode since this cathode shows the most uniform electron emission [6], and thus, the beam halo effect is clearly observed. The velvet cathode consists of 66% acetate and 34% nylon, and it is made by Youngdo Velvet, product # AW-1100.

The voltage is measured with a capacitive voltage divider near the diode, the total current is detected with a Rogowski coil, and the e-beam current is sampled with several Faraday cups by extracting beamlets through a 5 cm diameter aperture and B-dot probes as detectors. Figure 4 shows typical voltage and beam current density waveforms for 27 x 97 $cm^2$ velvet cathode experiments at 500 kV and an A-K gap of 5.2 cm. The current density in Fig. 4 has been obtained from a Faraday cup by dividing the measured current by the aperture cross-section.

## IV. TIME RESOLVED MEASUREMENTS

The edge of the electron beam is detected with a Faraday cup array that consists of 8 sensors with an area of 5 x 20 $mm^2$ each (see Fig. 5). They are electrically insulated from each other by 76 μm thick Kapton foils, and located on the anode plate. Pearson monitors, model # 2878, measure the collected current of each sensor with a sensitivity of 100 mV/A. The sensor array is placed 13 cm from the central vertical axis of the cathode. The array is positioned vertically so that the lowest sensor element is 3 mm above the cathode (not the beam) edge as shown in Fig. 5, line (a).

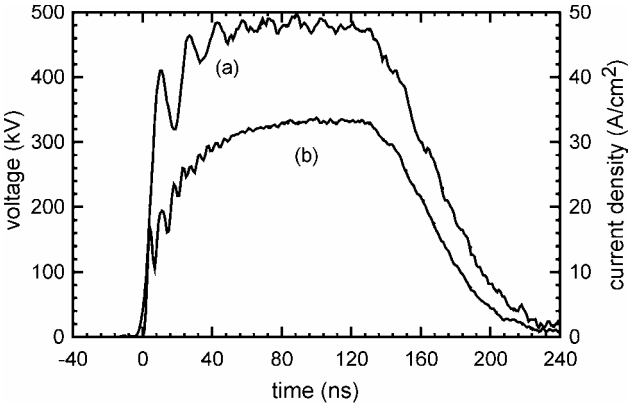


FIG. 4. Typical voltage and current density waveforms for velvet cathode experiments. (a) diode voltage and (b) current density waveform near the beam center, with an A-K gap of 5.2 cm, and t = 0 corresponds to the start of the current pulse.

Without an external magnetic field, the beam would pinch in its self-magnetic field. The applied magnetic field causes the beam to rotate and the *J*x*B* force associated with this rotation retards the pinch force. For small rotations, the rotation angle $\theta_r$ is given by [7]

$$\tan(\theta_r) = \frac{x}{z}\frac{B_y}{B_x} \qquad (1)$$

where $x$ is the beam propagation distance, $z$ is the cathode point horizontal coordinate, $B_y$ is the magnitude of the vertical component of the self-magnetic field, and $B_x$ is the applied magnetic field magnitude. Due to the current rise and fall the rotation angle varies in time, with its maximum value occurring at peak beam current. Lowering the external magnetic field amplitude results in a larger rotation angle as shown in Fig. 5, lines (b) and (c). In addition to the rotation, lower magnetic fields allow the beam to pinch more.

The Faraday cup array results are given in Figs. 6 and 7. The data has been normalized by the peak value of the current density measured at the top three sensors (6 to 8) for the case with $B_x$ = 1.4 kG. The beam halo is clearly detected by Faraday sensors 1 and 2 as shown in Fig. 6. The measured peak amplitude of 1.7 is not the peak of the normalized current density ($J_{peak}/J_{CL}$) since each sensor averages the current over a vertical height of 5 mm.

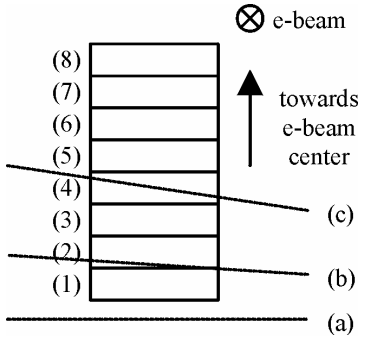


FIG. 5. Schematic of the Faraday cup array, overlaid with the position of the e-beam edge as measured by radiachromic film. (a) cathode edge with no rotation, (b) $B$ = 1.4 kG, and (c) $B$ = 0.6 kG. The faraday cups (1) to (8) each have a collector area of 5 mm x 20 mm.

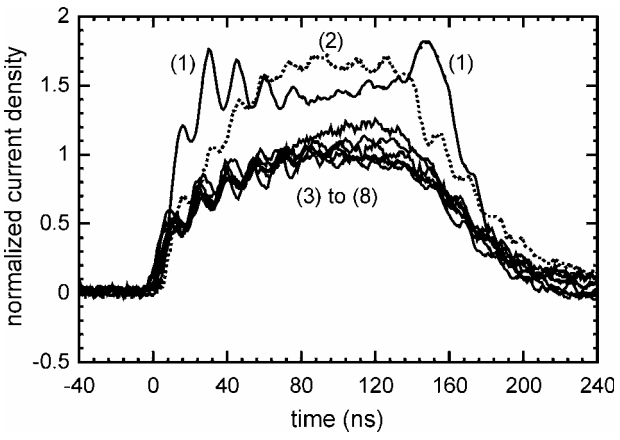


FIG. 6. Faraday cup array results with an external magnetic field of $B$ = 1.4 kG. The numbers (1) to (8) correspond to the traces of the individual faraday cups.

When the external magnetic field is lowered to 0.6 kG, the electron beam rotation angle is larger compared to the case with $B_x$ = 1.4 kG. In the middle of the current pulse, at t = 100 ns, the beam halo is located mostly over Faraday cup sensor 4. At that time, both sensors 1 and 2

do not carry any beam current. In addition, the results in Fig. 7 illustrate that during the risetime of the current, from t = 0 to 40 ns, the beam halo rotates through the bottom four sensors of the array as the self-magnetic field increases with beam current. The initial peak of sensor 2 at t = 17 ns, is approximately 2.5 times the signal amplitude of sensors 4 to 8, which indicates that the normalized current density of the beam halo ($J_{peak}/J_{CL}$) is at least 2.5 during the rise of the current pulse.

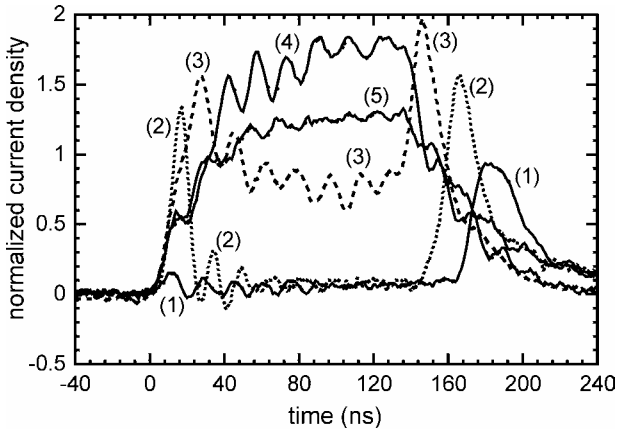


FIG. 7. Faraday cup array results with an external magnetic field of $B$ = 0.6 kG. The numbers (1) to (5) correspond to the traces of the individual faraday cups, and the waveforms of faraday cups (6) to (8) are not shown for clarity.

The low initial amplitude peak of sensor 1 at t = 10 ns indicates that the start of the electron emission at the cathode center is not significantly delayed compared to the emission of the cathode edge (i.e., the rotation angle increases rapidly during the initial overall current rise which suggests a large total beam current). The width of the beam halo can be approximated from individual peaks of sensors 1, 2 and 3 during the fall time of the beam pulse. At t = 146 ns, the signal of sensor 2 rises while sensor 3 has its maximum current signal. 20 ns later, at t = 166 ns, sensor 1 begins to rise while sensor 2 has its maximum current signal. These results indicate that the beam halo width should be on the order of the width of a single section of the Faraday cup array, which is 5 mm.

## V. 3-D SIMULATIONS

The electron beam propagation from the cathode to the anode has been simulated using the MAGIC 3-D PIC code for a 30 x 100 cm$^2$ cathode at 500 kV and with an A-K gap of 5 cm. The simulations show that the e-beam pinches both in the horizontal (z) and vertical (y) directions, rotates globally, and shears to some extent near the corners of the e-beam (see Fig. 8). The horizontal width decreases from 100 cm to 98.7 cm and 96.4 cm and the vertical height decreases from 30 cm to 29.1 cm and 27.6 cm, for an applied magnetic field of 1.4 kG and 600 G, respectively. Experimental data at 1.4 kG confirmed this trend with a 27 x 97 cm$^2$ cathode, which showed pinching by 1 cm each in width and height of the e-beam cross-section.

The beam distorts its rectangular shape (e.g., beam shear), which is seen by different horizontal and vertical rotation angles. Simulation show that the horizontal and vertical beam edges rotate by 1.3° and 2.5° at 1.4 kG, and 2.1° and 4.7° at 600 G, respectively. The shear is enhanced near the small vertical edges of the beam, which is due to the non-uniformity in the self-magnetic field amplitude as shown in Fig. 9. Neglecting the magnetic field from the return current and the beam halo, the self-magnetic field amplitude varies by approximately 10% from the corner of the beam cross-section (z = 50 cm, y = 15 cm) to the center of the vertical edge (z = 50 cm, y = 0 cm).

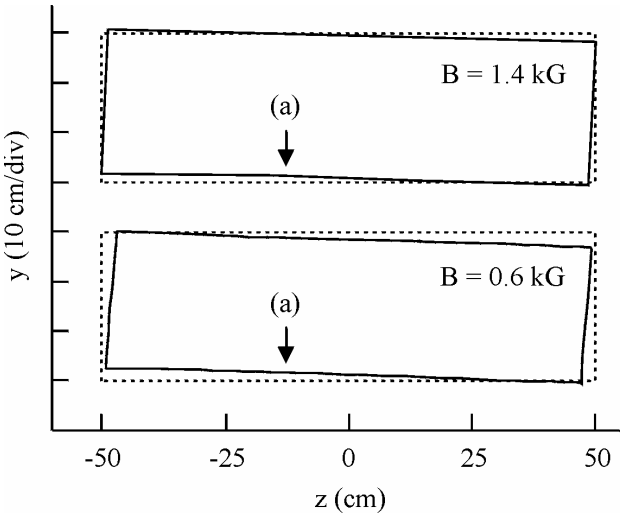


FIG. 8. 3-D PIC simulations showing electron beam rotation and pinching. The dashed line represents the dimensions of the cathode, and the solid lines illustrate the beam edge at the anode. The vertical e-beam displacement at position (a) is 1.1 cm and 1.8 cm for an external magnetic field of 0.6 and 1.4 kG, respectively. $V_{diode}$ = 500 kV, 30 x 100cm$^2$ cathode, and A-K gap = 5.0 cm.

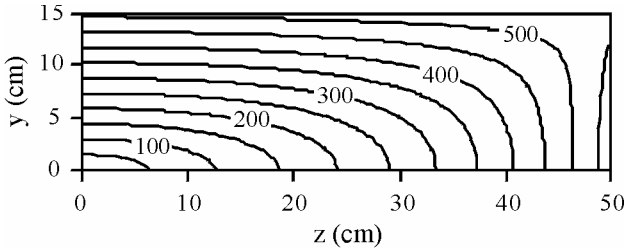


FIG. 9. Contour plot of the estimated self-magnetic field amplitude (in Gauss) in the first quadrant of the electron beam cross-section. For this calculation the current density is assumed to be uniform within the e-beam (without a beam halo), and magnetic field from the return current has been neglected. $V_{diode}$ = 500 kV, 30 x 100cm$^2$ cathode, and A-K gap = 5.0 cm.

Position (a) in Fig. 8 corresponds to the location of the Faraday cup array described in the previous section. The simulations show a vertical e-beam displacement at that position of approximately 1.1 and 1.8 cm for an external

magnetic field of 1.4 and 0.6 kG, respectively, compared to the experimental data of 0.8 and 2.0 cm (see Fig. 5). The simulations confirm that the time resolved vertical displacement of the beam halo as shown in Figs. 6 and 7 is due to both beam rotation and pinching.

## VI. SPATIALLY RESOLVED MEASUREMENTS

The time integrated spatial variation of the current density is measured with radiachromic (RC) film [8]. This measurement generates sub-millimeter spatial resolution over a large section of the electron beam (e.g., over the entire vertical height of the cathode and a horizontal width of 15 cm). The film, model number FWT-60-20S from Far West Technology, is sandwiched between two 25 μm thick titanium foils and placed 3 mm away from the anode. The metal foils prevent exposure of the RC film from ultraviolet photons and low energy plasma electrons. The relativistic electron beam passes through the titanium foil and exposes the RC film. This detector has been calibrated in-situ with adjacent faraday cups. Although the RC film is exposed by the total charge instead of the current density, the rise and fall times and the duration of the current pulse is almost constant for most cases, thus, it is valid to calibrate the film in terms of current density.

Figure 10 illustrates an example of RC film data with similar parameters as the PIC simulations presented in Sec. II. The simulations show a narrower current density peak than observed in the experiments. Discrepancies between simulations and RC film result from (i) the simplified modeling of the cathode edge in the simulations, and (ii) the simulations present an instantaneous beam halo where as the RC-film measures the time integrated current which includes beam rotation and slight beam pinching. The peak of the normalized current density ($J_{peak}/J_{CL}$) is approximately 2, and this result is a good representation of the beam halo for most parts of the edge (e.g., in some areas along the beam edge small hot-spots with current densities of up to 100 A/cm$^2$ are detected).

The method of recessing the cathode to eliminate the beam halo has been tested with a larger size cathode that fits directly into the cathode shroud. In that case, the cathode was recessed by 11 mm into the shroud and an electric field shaper was attached to the cathode edge with a similar configuration as shown in Fig. 1b. The single shot result shows that the beam halo can be eliminated at a reduced A-K gap voltage of 420 kV (see Fig. 11), at the expense of a broad edge. Furthermore, the polished aluminum field shaper showed considerable surface damage after 500 shots, when it was tested under repetitive operation at 5 Hz. During repetitive operation the field shaper eventually emits due to the high electric field strengths of more than 200 kV/cm at its surface (see Fig. 12).

In order to achieve a sharp rectangular current density profile, which is desired for the KrF laser, the field sharper should have a radius of a few millimeters (see Fig. 2). This leads to even higher electric fields on the surface of the field shaper as shown in Fig. 12, thus, a field shaper in a configuration as shown in Fig. 1b is not practical for repetitive high-voltage operation.

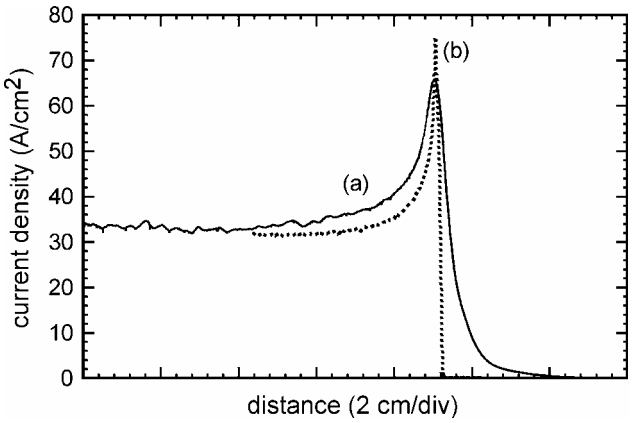


FIG. 10. Electron emission at the cathode edge without recess. (a) experimental results from a radiachromic film scan and (b) 2-D PIC code simulation with a 1 mm cell grid size. Experimental parameters are $V_{diode}$ = 500 kV, 27 x 97 cm$^2$ velvet cathode, and A-K gap = 5.2 cm.

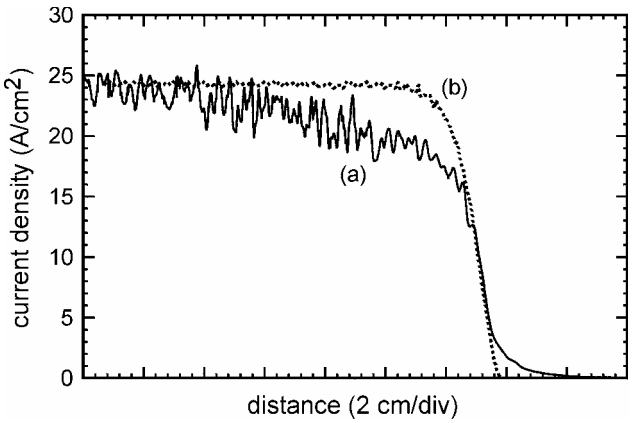


FIG. 11. Electron emission at the cathode edge with a 11 mm recess into the cathode shroud. (a) experimental results from a radiachromic film scan and (b) 2-D PIC code simulation with a 1 mm cell grid size. Experimental parameters are $V_{diode}$ = 420 kV, 35 x 106 cm$^2$ velvet cathode, and A-K gap = 5.2 cm.

## VII. STRIP CATHODE AND FLOATING FIELD SHAPERS

Currently, high-energy KrF laser systems are pumped with a large-area electron beam, which propagate from the vacuum diode through a hibachi into the laser gas cell [9-10]. Hibachi ribs support a thin pressure foil that separates the high-pressure laser gas from the diode vacuum. To achieve a high e-beam transmission efficiency into the laser gas, electron losses at the hibachi ribs must be minimized. One way of achieving this is to segment the cathode into strips as shown in Fig. 13. In order to eliminate the e-beam halos of each strip cathode, a new concept of a floating electric field shaper has been investigated. Instead of preventing electron emission from

a field shaper that is in direct contact with the cathode, the field shaper is electrically isolated from the cathode, and its capacitance and charge are minimized. Therefore, a floating field shaper is incapable of emitting large currents until the cathode plasma expands and electrically connects the field shaper to the cathode.

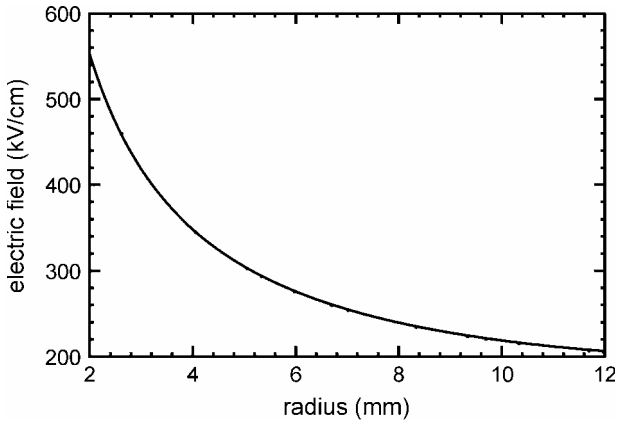


FIG. 12. Electrostatic field strength at the surface of a metallic electric field shaper as a function of its radius. The results have been approximated by a cylinder above a flat anode, with $V_{diode}$ = 420 kV, and a gap separation of 5.2 cm minus the radius of the field shaper.

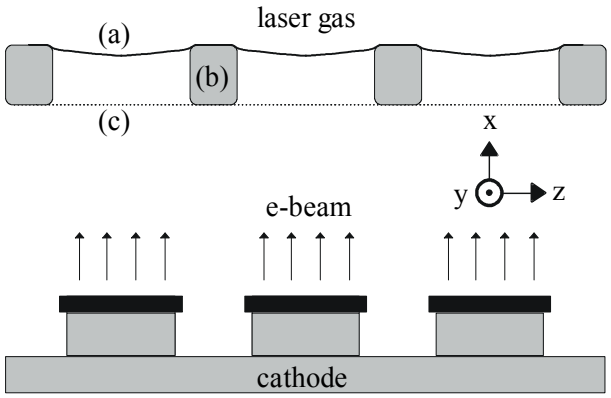


FIG. 13. Schematic of a diode with segmented strip cathode and hibachi. (a) pressure foil, (b) hibachi ribs, (c) optional anode foil.

The floating field shaper concept has been tested with a segmented strip cathode, with a strip width of 3.3 cm (1.3") and a strip separation of 7 mm (0.275") as shown in Fig. 14. For this test, the anode consisted of a Poco graphite plate covered by a 25 μm thick aluminized Kapton foil, as previously described in section III.

The spatially resolved time-integrated current at the anode (see Fig. 15) shows that without a field shaper the beam halo is 1.3 to 1.7 times the average current density measured in the middle of the cathode strip, and the electron beam is partially filling the gap between the cathode strips. With a floating field shaper both a decrease of the beam halo and less gap filling by the e-beam are seen. Without an electric field shaper, the beam halo is not as strong in this configuration compared to the factor of 2 in previous results (see Fig. 10). This is because the velvet strips are only separated by 7 mm so that space-carge from adjacent strips partially shield the edge electric field. Electrons emitted from the velvet strip edge will have a larger transverse velocity compared to electrons emitted from the middle of the strip because at the strip edge the electric field component $E_z$ is more dominant. The main portion of the strip beam decreases its width by approximately 1 mm due to self-pinching. A small portion of the beam electrons with higher transverse velocities spread by a few millimeters. With the field shaper, the electric field near the strip edge is decreased resulting in a smaller beam halo and lower average transverse velocity. The time integrated measurements in Fig. 15 show that the current density between to cathode strips is not zero. This effect is due to electron beam rotation during the rise and fall of the current pulse and due to some electrons with high transverse velocities.

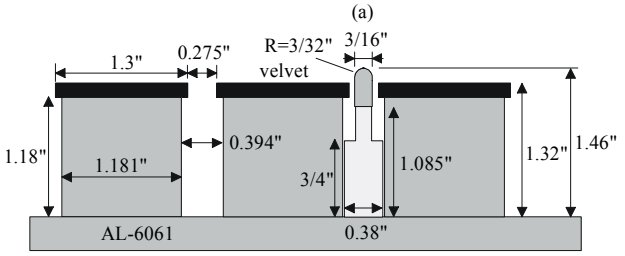


FIG. 14. Schematic of a segmented velvet strip cathode. Position (a) indicates the horizontal location of the floating field shaper made out of AL-6061-T6 that is bonded onto an acrylic spacer with superglue.

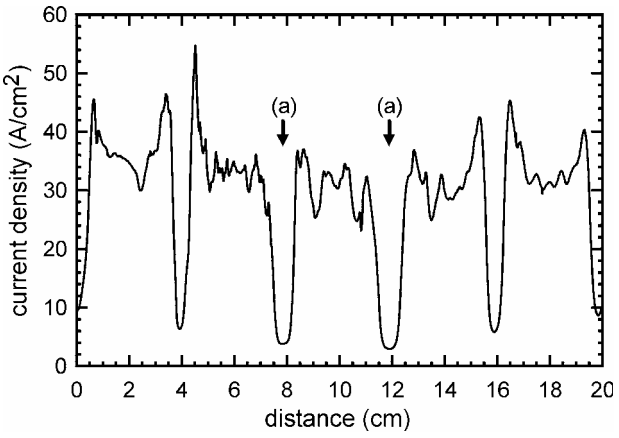


FIG. 15. Time integrated current results from a radiachromic film scan. Position (a) corresponds to the horizontal location of a floating field shaper as shown in Fig. 14. Experimental parameters are $V_{diode}$ = 500 kV, $I_{diode\ total}$ = 97 kA, B = 1.4 kG, outside cathode dimensions of 27.3 cm x 95.3 cm, and A-K gap = 4.8 cm.

The configuration shown in Fig. 14 has been tested under repetitive operation continuously at 1 pulse per second for 3000 shots at 500 kV, 160 ns FWHM pulse duration, and with an A-K gap of 4.8 mm. The RC film measurements on the 3001 shot showed almost identical results compared to the data presented in Fig. 15. The

floating field shaper did not show any visible surface damage after more than 3000 shots compared to the significant surface damage found after only 500 shots on the field shaper that is in direct contact with the cathode.

The strip cathode configuration has been modified to incorporate parameters of a hibachi with 1 cm wide ribs and 4 cm rib-to-rib spacing. The cathode strip spacing is increased to 4.04 cm (1.592") and the strips are rotated by 4° to compensate for beam pinching and beam rotation. Figure 16 shows two field shaper designs that have been tested: (a) a narrow field shaper with the same dimensions as in the previous configuration, and (b) a wide field shaper. The results are provided in Figure 17, which indicates that without a field shaper, the beam halo is more pronounced due to the larger cathode strip separation. The narrow field shaper significantly reduces the beam halo where as the wide field shaper is not as effective. The narrow field shaper is likely to produce of larger changes of the electric field at the beam edge and it is placed slightly closer to the velvet cathode compared to the wide field shaper.

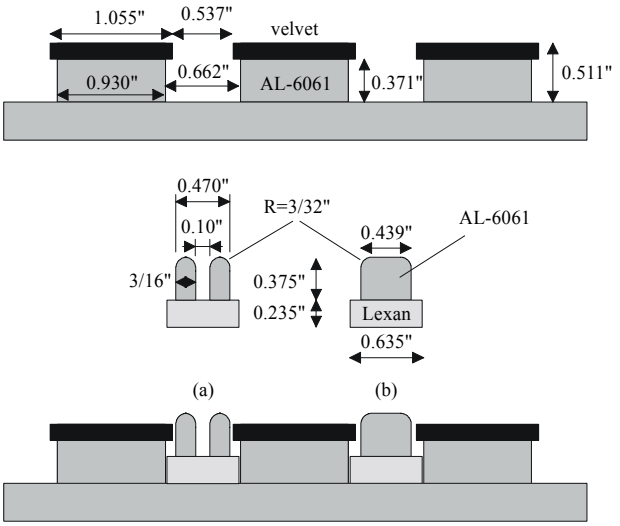


FIG. 16. Schematic of a segmented velvet strip cathode with wider strip separation. Positions (a) and (b) indicate the horizontal location of the narrow and wide field shapers. The entire cathode consists of 24 emitting strips, each with an area of 2.7 cm x 27.2 cm.

With the narrow field shapers, the average current density of the strip is approximately 60 A/cm$^2$, and the beam halo is eliminated (see Figure 17, at position 6 cm). The current density amplitude is significantly higher the expected Child-Langmuir current density for a large area cathode, which should be 40.6 A/cm$^2$ for an A-K gap of 4.2 cm and a diode voltage of 455 kV. This current density increase is predicted from simulations and an analytical approximation by Lugisland *et al*. [11] and Lau [12] when there is no beam halo. For narrow cathode widths, the current density is estimated by [12]

$$J \cong \left(1 + \frac{d}{\pi w}\right) J_{CL} \qquad (2)$$

where d is the distance of the A-K gap and w is the width of the cathode. This approximation assumes a constant current density along the cathode width (e.g., without beam halos). For the parameters of this experiments, this theory predicts a current density that is 1.5 times larger than $J_{CL}$, which is in good agreement with the measured data. Strong beam halos limit the current density in the middle of the strips as shown in Fig. 17, position 22 cm. The numerical approach by Watrous *et al*. [13] that solves Poisson's equation and determines a current density profile of a single strip cathode with beam halos also estimates lower current densities in the middle of a strip compared to the analytical approximation by Lau [12] that neglects the beam halo.

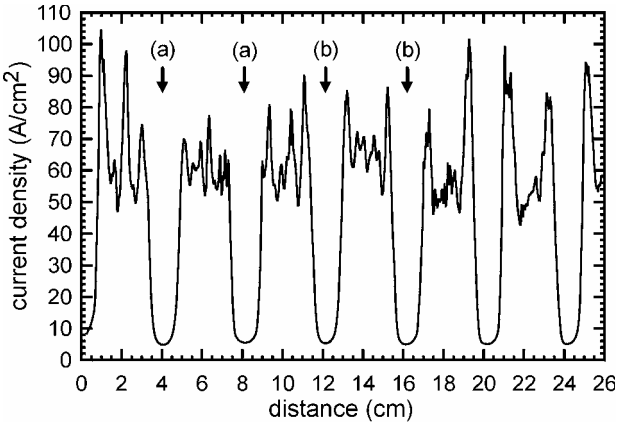


FIG. 17. Time integrated current results from a radiachromic film scan. Positions (a) and (b) correspond to the horizontal location of a floating field shaper as shown in Fig. 16. Experimental parameters are $V_{diode}$ = 455 kV, $I_{diode\ total}$ = 110 kA, B = 1.4 kG, and A-K gap = 4.2 cm.

The strip cathode shows that the current density uniformity of narrow cathodes is inferior to large area cathodes (see Figure 10). A possible explanation relates to the expected non-uniformities in the electric field. For a large area cathode the electric field is strongly non-uniform only in the beam halo regions. With a narrow strip cathode the non-uniformities of the electric field in the diode box are significantly increased. Future work will investigate the current density non-uniformities of cathode strips and test the floating field shaper concept on a large area strip cathode.

## VIII. SUMMARY

The electron beam halo of large area cathodes has been measured and simulated. Recessing the cathode into the shroud reduces the electric field at the cathode edge and reduces or eliminates the beam halo. This concept works for single shot operation, but with electric fields that exceed 100 kV/cm, continuous elimination of the beam halo is unrealistic without emission from the field shaper. By electrically insulating the field shaper from the cathode, emission from the field shaper can be significantly minimized or eliminated during repetitive

operation at pulse durations of 160 ns. Although the electron beam uniformity is reduced to some extent, this novel concept eliminates the beam halo.

## ACKNOWLEDGMENTS

This work is supported by the US Department of Energy.

## REFERENCES

[1] J.R. Pierce, "Theory and design of electron beams," 2nd ed. New York: D. Van Nostrand Company, 1954.

[2] J.D. Sethian, et al., "Pulsed power for a rep-rate, electron beam pumped KrF laser," IEEE Trans. Plasma Sci., vol. 28, pp. 1333-1337, Oct. 2000.

[3] J.D. Sethian, et al., "The Electra laser program," Proc. IEEE Pulsed Power Plasma Science Conference, Las Vegas, NV, June 17-22, 2001.

[4] B. Goplen, L. Ludeking, D. Smithe, and G. Warren, "User-configurable MAGIC for electromagnetic PIC calculations," Computer Physics Communications, vol. 87, pp. 54-86, May 1995.

[5] J.J. Watrous, J.W. Lugisland, and G.E. Sasser, "An improved space-charge-limited emission algorithm for use in particle-in-cell codes," Phys. Plasmas, vol. 8, pp. 289-296, Jan. 2001.

[6] M.C. Myers, et al., "Development of a durable, large area cathode for repetitive, uniform electron beam generation," IEEE Pulsed Power Plasma Science Conference, Las Vegas, NV, June 17-22, 2001.

[7] L.A Rosocha and K.B. Riepe, "Electron-beam sources for pumping large aperture KrF lasers," Fusion Technology, vol. 11, pp. 576-611, May 1987.

[8] K.C. Humpherys and A.D. Kantz, "Dosimetry and quality control in electron beam processing," IEEE-Transactions on Nuclear Science, vol. ns-26, 1979, pp. 1784-1789.

[9] J.D. Sethian, S.P. Obenschain, K.A. Gerber, C.J. Pawley, V. Serlin, C.A. Sullivan, W. Webster, A.V. Deniz, T. Lehecka, M.W. McGeoch, R.A. Altes, P.A. Corcoran, I.D. Smith-ID, and O.C. Barr, "Large area electron beam pumped krypton fluoride laser amplifier [Nike ICF laser]," Review-of-Scientific-Instruments. vol. 68, pp.2357-2366, 1997.

[10] I. Okuda, J. Ma, E. Takahashi, I. Matsushima, Y. Matsumoto, S. Kato, Y. Owadano, "Initial testing of a high-repetition-rate electron-beam-pumped KrF laser amplifier," Applied Physics B (Lasers and Optics), vol. B72, pp. 623-626, 2001.

[11] J.W. Luginsland, Y.Y. Lau, and R.M. Gilgenbach, "Two-Dimensional Child-Langmuir Law," Physical Review Letters, vol. 77, pp. 4668-4670, 1996.

[12] Y.Y. Lau, "Simple Theory for the Two-Dimensional Child-Langmuir Law, Physical Review Letters, vol. 87, pp. 278301_1-278301_3, 2001.

[13] J.J. Watrous, J.W. Luginsland, and M.H. Frese, "Current and current density of a finite-width, space-charge-limited electron beam in two-dimensional, parallel-plate geometry," Physics of Plasmas, vol. 8, pp. 4202-4210, 2001.